JOURNAL OF MATERIALS SCIENCE 23 (1988) 1886–1894

Experimental verification of a microbuckling model for the axial compressive failure of high performance polymer fibres

STEVEN J. DeTERESA*, ROGER S. PORTER, RICHARD J. FARRIS
Polymer Science and Engineering Department, University of Massachusetts, Amherst, Massachusetts 01003, USA

A previously derived theoretical compressive strength for fibres composed of uniaxially oriented and extended polymer chains was compared with the measured strengths of several high performance fibres. For failure initiated by elastic microbuckling of polymer chains or fibrils, the maximum fibre strength is predicted to be equal to the minimum longitudinal shear modulus of the fibre. An excellent linear correlation between measured strengths and torsion moduli was obtained for four liquid-crystalline polymer fibres and high modulus graphite fibres. The correlation shows that measured strengths are 30% of the corresponding torsion moduli for all these fibres. A high modulus, high strength polyethylene fibre exhibited a compressive strength–torsion modulus ratio that was lower than the value 0.3 obtained for the other fibres examined in this study.

1. Background

The axial compressive failure of high-performance polymer fibres is manifest by the formation of kink bands [1–6]. Compressive kink bands have been observed to form in many anisotropic materials and structures (see references in [7]). Where the stages of kink band formation were studied, it was concluded that the bands nucleate locally and then propagate through the material [4, 8–19].

Independent studies of kink band nucleation in oriented polymers [19], card decks [12] and rubber laminates [13] revealed that local material buckling precedes the collapse into a propagating kink band. Indeed, it is remarkable that the schematic representations of the process of kink band nucleation presented in each diverse study are virtually identical. An example of these representations is shown in Fig. 1. These observations suggest that an estimate of the compressive strength of anisotropic materials that form compressive kink bands may be obtained from an elastic microbuckling analysis.

A theoretical compressive strength for high performance polymer fibres has been calculated by the authors using an elastic buckling analysis. A simple model for a collection of uniaxially-oriented and laterally-interacting extended polymer chains has been employed [7]. Assuming that the degree of interchain interaction can be characterized by the transverse and shear moduli of the fibre, the following estimate of fibre compressive strength, σ_c, was obtained

$$\sigma_c = -G \quad (1)$$

where G is the longitudinal shear modulus of the fibre.

This simple prediction of compressive strength was obtained, in part, by assuming the fibres to be composed of high molecular weight extended polymer chains. Given this assumption, it can be demonstrated that Equation 1 is the critical buckling condition for several simple buckling patterns, some of which are depicted in Fig. 2. Comparison of the pattern shown in Fig. 2c with those observed in the nucleation region of a kink band (Fig. 1) clearly shows the validity of the deformations used in the microbuckling analysis to calculate a theoretical fibre compressive strength. The accuracy of this theoretical value is examined in the present study by comparing measured compressive strengths with longitudinal shear moduli for six high performance fibres.

2. Experimental details

Of the six fibres examined, three had been spun from anisotropic solutions of lyotropic liquid crystalline polymers by the dry jet–wet spinning process [20]. These include poly(*p*-phenylene terephthalamide) (PPTA), poly(*p*-phenylene benzobisthiazole) (PBT) and poly(2,5-benzoxazole) (ABPBO). All three fibres were tension heat-treated after spinning to improve orientation and thereby increase axial modulus. Kevlar 49 was the PPTA fibre selected for this study.

A fibre melt-spun from an anisotropic melt of a thermotropic liquid crystalline polymer was also examined. This fibre is a nematic thermotropic polyester (NTP) produced by Celanese Co. and it was also subjected to tension heat-treatment after spinning. The chemical structures of all four liquid crystalline polymers are shown in Fig. 3.

**Present address*: Ceramic and Polymer Composite Group, Chemistry and Materials Science Department, Lawrence Livermore National Laboratory, University of California, PO Box 808, Livermore, California 94550, USA.

0022–2461/88 $03.00 + .12

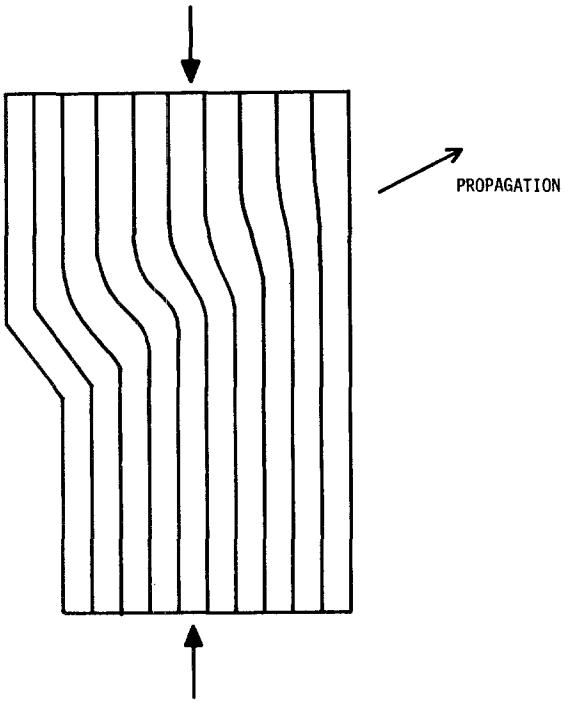

Figure 1 Representation of kink band formation.

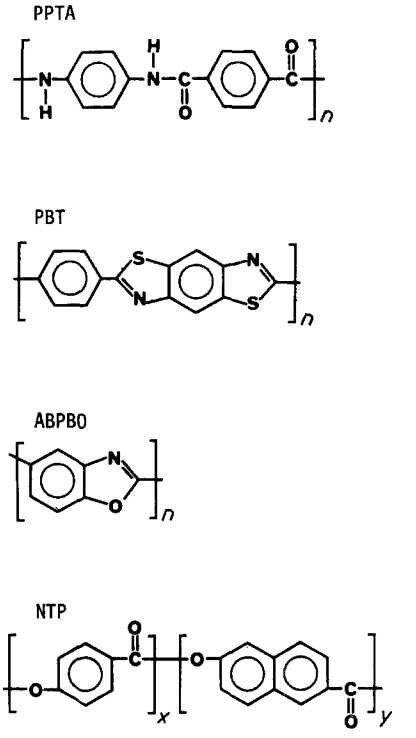

Figure 3 Chemical structures of liquid-crystalline polymer fibres.

A high modulus/high strength polyethylene fibre produced by the gel-spinning process [21] was obtained from the Allied-Signal Co.

The sixth type of fibre tested was a high modulus graphite fibre (Union Carbide P-75) spun from a mesophase pitch. This fibre was stretched during the graphitization process to improve orientation and therefore axial modulus [22, 23]. Graphite fibres were included in this study of fibre axial compressive strengths because their structure generally consists of axially oriented microfibrillar graphite ribbons having the crystalline graphite basal plane parallel to the long axis of the ribbons [22]. In terms of the model proposed for the extended-chain polymers, the graphite fibre structure can be modelled with laterally-interacting extended graphite sheets that are permitted to buckle under compression.

The reasons for selecting a particular graphite fibre are two-fold. First, studies of the compressive behaviour of graphite fibres show that compressive buckling or kinking only occurs in fibres that have a well-developed and well-oriented graphitic structure [8, 24]. These fibres are typically produced by heat-treatment to temperatures near 2800° C and usually exhibit the highest tensile moduli measured for carbon fibres. Second, the P-75 fibre appears to have a well-developed radial structure, i.e. the graphite basal planes are oriented predominantly parallel to fibre radii (see Fig. 4). Therefore, the torsion modulus for such fibres should be nearly equal to the shear modulus for deformation between graphite basal planes. This shear modulus is thus the theoretical estimate of axial compressive strength for graphite fibres that fail due to the microbuckling of extended graphite sheets.

The diameter of fibre samples was measured at several locations along each sample length. The cross-sections of all fibres except PE were circular.

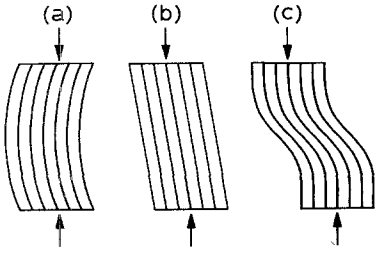

Figure 2 Potential microbuckling deformations for a collection of long, extended polymer chains. (Each line represents a single chain.)

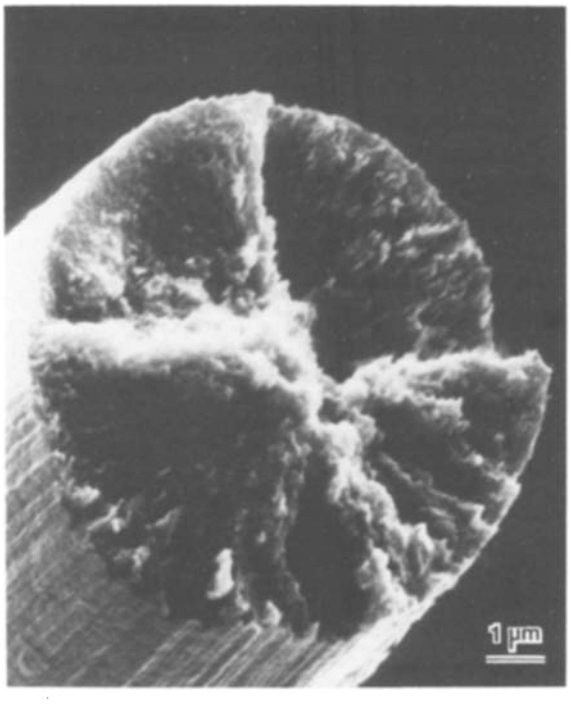

Figure 4 Scanning electron micrograph of the tensile fracture surface of P-75 graphite fibre.

Therefore, with the exception of PE, all diameters were measured using a laser diffraction technique [25] that yielded values with a precision of $\pm 2\%$.

The PE fibres had an irregular cross-section that varied significantly along sample lengths. The area and shape of each PE fibre sample were determined, after testing, at several locations along the length by embedding the fibre in a microtome resin followed by cutting transverse sections for examination using light microscopy. Micrographs of sections cut from locations ~ 2 mm apart along the fibre length were used to determine the cross-sectional area of the fibre by a paper-weighing technique.

Fibres were mounted on to cardboard tabs with epoxy for mechanical testing. Tensile tests were performed on samples with gauge lengths ranging from 2 to 8 cm in order to correct for machine compliance effects [26]. Tensile properties of PE and P-75 graphite fibres were obtained from the manufacturers.

The torsion modulus of the fibres was measured using a free torsion pendulum [1]. The equation for calculating the torsion modulus from measurements of underdamped torsional oscillations of a fibre with circular cross-section is given by

$$G = \frac{8I_d l}{\pi\tau^2 r^4}\left[\pi^2 + \frac{(\ln \Delta)^2}{16}\right] \quad (2)$$

where I_d is the polar moment of inertia of disc pendulum, l the sample length, τ the period of oscillation, r the fibre radius, and $\ln \Delta$ the logarithmic decrement of amplitude.

Torsion pendulum tests were performed at ambient conditions, and damping was noticeable for every fibre tested. However, all values of Δ were found to be > 0.5 and therefore, as readily verified from Equation 2, the damping had a negligible effect on the calculated torsion modulus. Hence, the torsion modulus was determined with sufficient accuracy using

$$G \simeq \frac{8\pi I_d l}{\tau^2 r^4} \quad (3)$$

Fibre samples 2 cm long were set into torsional oscillation by manually twisting the disc pendulum and then carefully releasing it. This initial twist never exceeded a fibre surface shear strain of 0.5%. The period of oscillation was measured by timing the motion of a mark on the disc pendulum relative to a marked position on a stationary platform placed just beneath the oscillating pendulum.

Two clamp-type aluminium gear blanks were used as disc pendulums. The polar moments of inertia of the gear blanks were calculated to be 50.3 and 354 g mm^2 using dimensions measured with a micrometre (accurate to 1 μm) and weights measured with an analytical balance. The accuracy of these measurements was checked by calculations for the density of aluminium, giving 2.71 and 2.72 g cm^{-3}, in excellent agreement with the actual density of 2.669 g cm^{-3}. The large pendulum was used for the PE fibre tests and the small one for all other fibre tests.

The fibre axial compressive strengths were calculated from the product of the compressive strain to kink band formation and the axial tensile modulus.

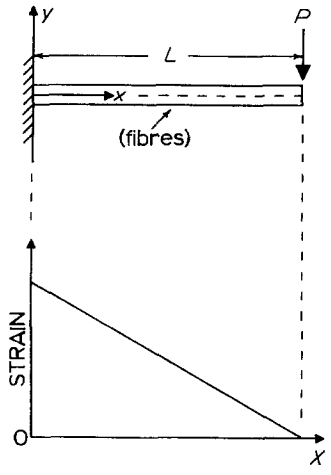

Figure 5 Longitudinally distributed axial normal strains in an elastic beam loaded in cantilever bending.

This calculation is based on the assumptions that the fibres are linear-elastic up through the compressive strain for initiation of kink bands and that the axial tensile and compressive moduli are identical. The critical compressive strains to kink band formation were measured using a variation of the beam bending technique described previously [1]. In the tests performed here, fibres bonded to the surface of thick transparent elastic beams were compressed by bending the beam in a cantilever mode. This bending configuration results in a linear distribution of longitudinal compressive (and tensile) strains along the beam length as shown in Fig. 5.

Fibres were examined in the compressed state by holding the beam in the bent configuration while making observations with an optical microscope. A schematic diagram of a simple rig built for this purpose, which sits on the stage of the optical microscope, is shown in Fig. 6.

Fibres were mounted under slight tension (0.5 g) on to the surface of 0.5 in. $\times$ 0.25 in. $\times$ 6 in. (~ 1.28 cm $\times$ 0.65 cm $\times$ 15.25 cm) Lucite® beams, parallel to the length of the beams, by applying several coats of Krylon® acrylic spray. Fibres were tested after allowing the acrylic coating to dry to a hard film. It is emphasized that any shrinkage of the film during drying, which might put residual compressive stresses on the bonded fibres, is prevented by using only a thin acrylic coating on a relatively thick beam.

After a beam with bonded fibres was clamped in the rig as shown in Fig. 6, a circular wedge was inserted between the beam and the base plate of the rig to deflect the beam. Bonded, compressed fibres were examined *in situ* using a transmission light microscope. A wedge of known diameter, v, was inserted at a distance, L, measured from the clamped end of the beam. The distance, d, from the clamped end to the point along the compressed fibre length where the last kink band was seen was measured. The compressive strain in the fibre at any point x measured from the clamped end is assumed to be equal to the surface strain $\varepsilon(x)$ of the bent beam at the same location. This strain is calculated from

$$\varepsilon(x) = \frac{3tv}{2L^2}\left(1 - \frac{x}{L}\right) \quad (4)$$

TABLE I Tensile properties of fibres

Fibre	Diameter range (μm)	Modulus ± S.D. (GPa)	Break strength ± S.D. (GPa)
PPTA	11.4–12.8	123 ± 5.7	3.2 ± 0.16
PBT	12.4–13.5	265 ± 15	2.6 ± 0.20
ABPBO	13.2–18.1	120 ± 10	3.0 ± 0.55
NTP	18.7–26.1	77 ± 2.9	3.2 ± 0.64
PE	(38)*	117*	2.6*
P-75	9.7–10.0	500*	2.0*

*Manufacturer's data.

where t is the thickness of the beam. The critical compressive strain, ε_c, for kink band formation is defined as the strain at $x = d$.

The compressive strain distribution in the fibre could be changed either by using a larger diameter wedge or by moving the wedge closer to the clamped end of the beam (i.e. reducing L). In this manner, the remaining undamaged (unkinked) regions of the bonded fibre could also be tested to determine ε_c. Thus, several determinations of ε_c were obtained from one length of fibre. Because the compressive strain for kink band formation was measured, fibres with an irregular cross-section, such as the gel-spun PE, could be tested with the same accuracy as fibres having circular cross-sections.

Equation 4 is derived from linear beam theory, which is based on the assumption of small curvatures for bent beams. Therefore, in all tests performed here, wedges of relatively small diameter were held at comparatively large distances L so that use of Equation 4 to calculate ε_c would be valid.

The morphology of fibres kinked under compression was examined using scanning electron microscopy (SEM) and optical microscopy. Kinked fibres were prepared for microscopic observations by using a matrix shrinkage technique for fibre compression [27]. This technique involves the compression of single fibres due to the shrinkage of a surrounding nylon-6 matrix as it is cast from a formic acid solution. Compressed fibres were recovered from the matrix by redissolving the nylon with formic acid.

Tensile tests were performed at strain rates of $\sim 5 \times 10^{-4}\,\text{sec}^{-1}$ using an Instron Universal Testing Machine. A polarizing Zeiss optical microscope was used to examine fibres bonded to bent beams. The surfaces of fibres before and after compression were examined using an ETEC Autoscan SEM.

3. Results

The range of diameters and the tensile properties measured for each fibre are listed in Table I. Fibres that are produced in large quantities, namely PPTA (Kevlar 49), PBT and P-75 graphite, exhibited relatively uniform diameters along sample lengths. The filament-to-filament variation in diameter for these three fibres was relatively small. The ABPBO and NTP fibres were produced by laboratory-scale spinning processes and were found to exhibit large variations in diameter, both along the length of a filament and between individual filaments.

Each type of fibre is one variant of a family which exhibits a wide range of tensile properties that depend on spinning and post-heat-treatment conditions. The fibres used in this study were selected because they exhibit some of the best tensile properties attainable for their respective class of organic material. Although the moduli of these materials cover a range of values, the tensile strengths are all surprisingly similar. The coefficients of variation of tensile strengths ranged from 10 to 20%. All fibres, except PE, exhibited a linear stress–strain behaviour to break. Consequently, a reasonable estimate of strain at break for these fibres is simply the ratio of tensile strength to tensile modulus.

A 2 cm length of PE fibre was tensile-tested to a load below break. This fibre exhibited tensile yield behaviour. After testing, the intact fibre was embedded in resin and sectioned to determine the shape and area of the cross-section. The profiles of two transverse sections of this sample taken approximately 1 cm apart are illustrated in Fig. 7a. The cross-sectional area was measured to be $1.1 \times 10^3\,\mu\text{m}^2$. Assuming that the fibre "diameter" supplied by the manufacturer was calculated from linear density measurements, this hypothetical diameter would correspond

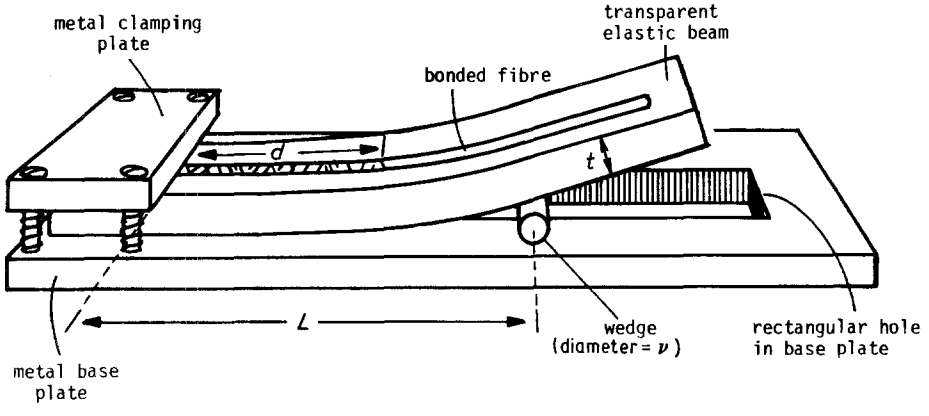

Figure 6 Schematic illustration of the apparatus used to determine critical compressive strain for kink band formation in single fibres.

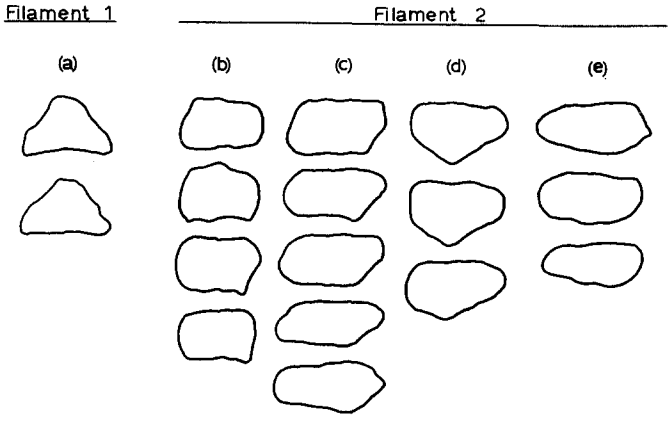

Figure 7 Tracings of optical micrographs of transverse sections of PE fibres. (a) Filament 1: tensile test samples. (b to e) Filament 2: torsion test samples.

to a cross-sectional area of $1.13 \times 10^3 \mu m^2$. Therefore, the areas calculated from micrographs of transverse fibre sections are in excellent agreement with the manufacturer's data.

Using a machine compliance value obtained from tensile tests of other fibres under the same test conditions, a tensile modulus of 110 GPa was calculated for the single PE sample tested. Within experimental error, this value is identical to the tensile modulus of 117 GPa quoted by the manufacturer. The limit of proportionality (onset of yielding) occurred at a tensile stress of 170 MPa.

Values of torsion modulus, G, critical compressive strain, ε_c, and calculated axial compressive strength for each fibre are given in Table II. Axial compressive strengths of PPTA (Kevlar 49) [28] and PBT [29] fibres were also obtained by calculating the stress in each fibre at the reported yield or failure load, measured in longitudinal compression, of unidirectional composites of these fibres. These values are also listed in Table II.

It was discovered that axial tensile stresses resulted in an apparent increase in the fibre torsion modulus that is given by the equation

$$G^* = -c\sigma + G \quad (5)$$

where σ is the axial tensile stress, G^* is the apparent torsion modulus, G is the true torsion modulus and c is a constant approximately equal to -0.75. The reasons for, and implications of, this effect will be examined in a future publication. For the present, it is sufficient to consider the increase in measured torsion modulus due to the axial stress generated by the weight of the disc pendulum. Accordingly, the corrected values of torsion modulus for each fibre are given in Table II. For thinner fibres, this correction for pendulum weight amounted to $\leqslant 10\%$.

The measured torsion modulus of the P-75 graphite fibre is close to the value of 4.1 GPa reported for the inter-basal plane shear modulus of a dislocation-free graphite crystal [30]. The similarity of these shear moduli is evidence for a radial structure in P-75 graphite fibres.

The largest degree of uncertainty in torsion modulus is for PE fibres, because of their irregular and varying cross-sections. The profiles of cross-sections of four test specimens (all 2 cm long) are shown in Figs 7b to e. The torsional rigidities of these specimens were calculated assuming that the cross-sectional profiles could be approximated by an ellipse, rectangle or triangle, whichever fit most closely the particular profile. It should be noted that all four specimens were cut from a single filament approximately 12 cm long, and an examination of Figs 7b to e clearly shows the variation of the PE fibre cross-section along the length of an individual filament. Although the coefficient of variation of the torsion modulus for PE fibres is large, the mean value of 0.7 GPa is in good agreement with the torsion modulus of 0.6 GPa measured for hot-drawn PE monofilaments [31].

In previous studies it was shown that PPTA (Kevlar 49) fibres form helical kink bands under axial compression [1, 27]. SEM and optical micrographs of kink bands in PBT, ABPBO, NTP and PE fibres are shown in Figs 8 to 11. Except for the PE fibre, no kink bands were observed in fibres prior to axial compression. Considering the relative thickness of the PE fibre and its low critical strain to kink band formation, the few kinks seen in the as-received fibre probably resulted from fibre bending due to handling.

Kink bands initiate in PBT fibres as thin bands oriented at $\sim 70°$ to the fibre axis. The arrow in Fig. 8 points to an incipient band. At higher levels of

TABLE II Torsion moduli and compressive strengths of fibres

Fibre	Torsion modulus ± S.D. (GPa)*	Critical compressive strains ± S.D. (%)†	Calculated compressive strengths ± S.D. (GPa)	Composite compressive strength (GPa)‡
PPTA	1.5 ± 0.20	−0.50 ± 0.03	−0.62 ± 0.06	−0.45 [28]
PBT	1.2 ± 0.14	−0.10 ± 0.02	−0.27 ± 0.08	−0.31 [29]
ABPBO	0.62 ± 0.07	−0.18 ± 0.03	−0.21 ± 0.06	
NTP	0.45 ± 0.04	−0.15 ± 0.01	−0.12 ± 0.01	
PE	0.7 ± 0.22	−0.08 ± 0.015	−0.09 ± 0.02	
P-75	5.6	–	−1.3 to −2.0 [8, 24]	

*Corrected for pendulum weight.
†Corrected for tensile prestrain applied during mounting to beam.
‡Calculated from σ_c/V_f, where σ_c = longitudinal compressive strength of composite, V_f = fibre volume fraction of composite.

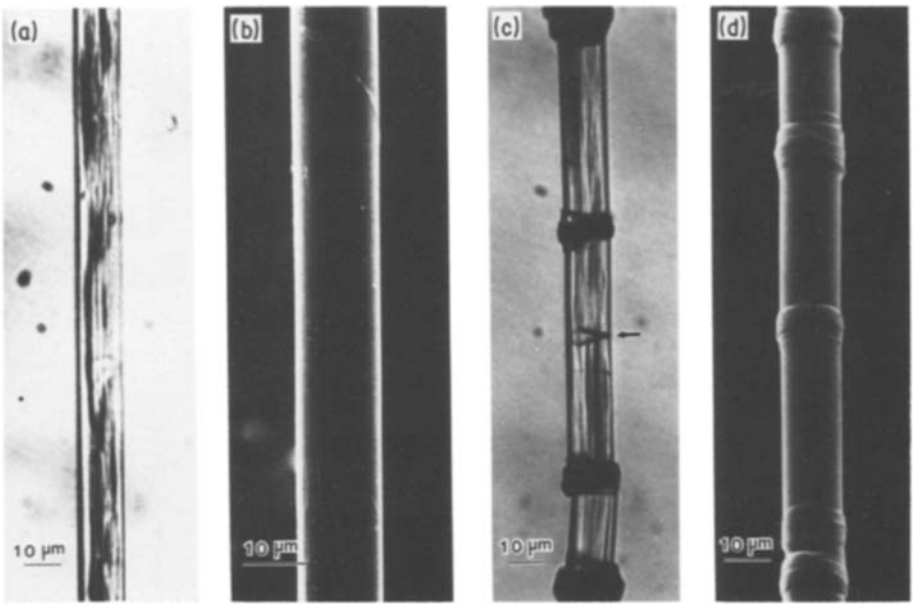

Figure 8 PBT fibre. Before compression: (a) optical micrograph, (b) scanning electron micrograph. After compression: (c) optical micrograph, (d) scanning electron micrograph.

compressive strain, the bands propagate across the fibre and eventually form the thick, bulging perpendicular deformation bands seen in Figs 8c and d. These large bands form at periodic intervals along the fibre axis.

The kink bands in compressed ABPBO fibres shown in Figs 9c and d bear some resemblance to the helical kink bands observed in PPTA fibres. Like the PPTA kink bands, the bands in ABPBO fibres are oriented at angles ranging from 50 to 60° to the fibre axis. Although the ABPBO compressive kink bands appear to be helical, there is no propagation of any one helical band for any appreciable distance along the fibre length.

In optical micrographs of compressed NTP fibres (Fig. 10c), black deformation bands of various thicknesses are observed to be oriented at $\sim 55°$ to the fibre axis. Where two such bands criss-cross, the fibre exhibits bulging that is similar to the dilatation in the deformation bands of PBT fibres. The surface of compressed NTP fibres exhibits kink bands oriented at several angles to the fibre axis (Fig. 10d). There is no obvious regularity to the spacing of these bands along the length of NTP fibres.

Compressed PE fibres exhibit both obliquely oriented kink bands and bands that are oriented at 90° to the fibre axis (Figs 11c and d). In many regions of compressed PE fibres, deformation bands formed at regular intervals along the fibre axis.

The graphite fibre is opaque and thus could not be measured for compressive strength using transmission optical microscopy with the beam bending technique. However, the compressive strengths of similar pitch-based graphite fibres were calculated by other workers who used the elastica test to measure the compressive stress that initiated inelastic behaviour [24] and an axial compression test to measure critical compressive strains [8]. The compressive strengths calculated in both studies correspond to the axial compressive stress in the fibre at the onset of localized kinking. The

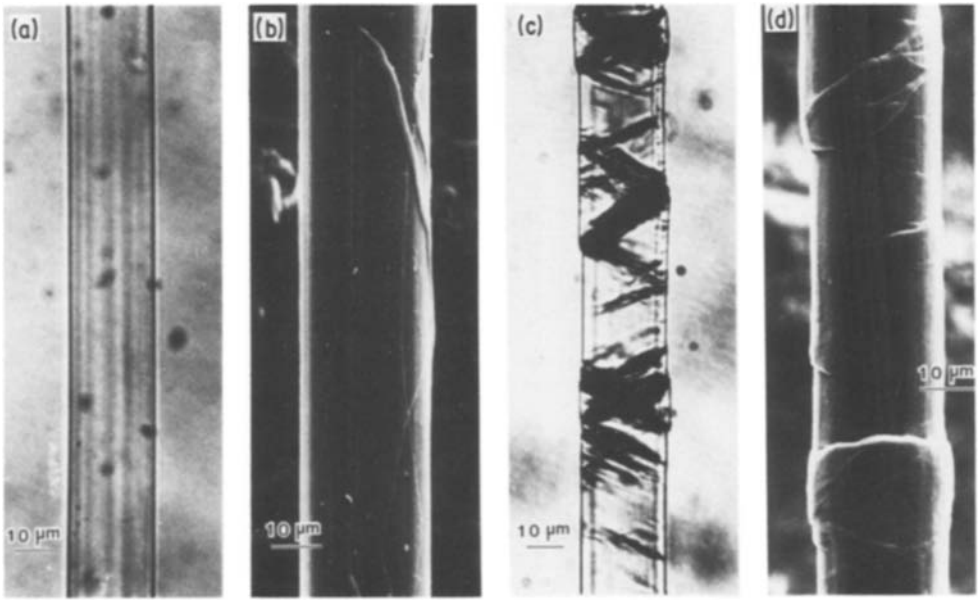

Figure 9 ABPO fibre. Before compression: (a) optical micrograph, (b) scanning electron micrograph. After compression: (c) optical micrograph, (d) scanning electron micrograph.

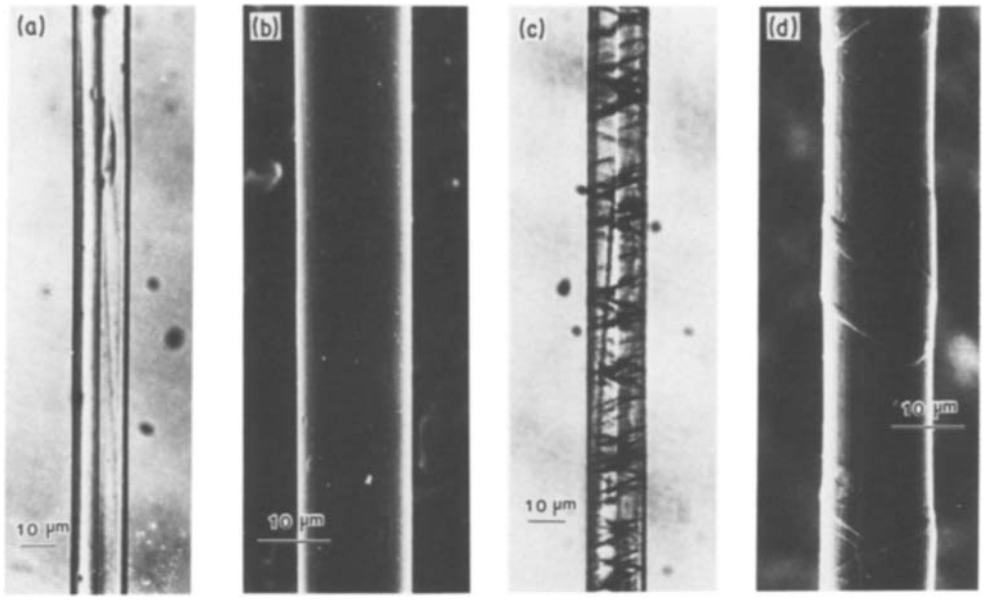

Figure 10 NTP fibre. Before compression: (a) optical micrograph, (b) scanning electron micrograph. After compression: (c) optical micrograph, (d) scanning electron micrograph.

kinking appeared on the fibre surface in the form of a deformation band oriented at 90° to the fibre axis. The range of compressive strength obtained for graphite fibres in these studies is given in Table II.

The relatively large degree of uncertainty in compressive strengths that were calculated from the product of tensile modulus and critical compressive strains arises from the combined errors in these latter two quantities. However, the range of variation in compressive strengths is of the same order as the range of uncertainty in the tensile strengths.

A comparison of measured compressive strengths with the predicted critical stresses for elastic instabilities, i.e. torsion moduli, is shown in Fig. 12. The correlation between these quantities is extremely good for all fibres except PE. The values for PPTA, PBT, ABPBO and NTP fibres can be fitted to a straight line with correlation coefficient $r = 0.89$. If the compressive strengths of PPTA and PBT fibres calculated from composite data are used for the linear correlation, the goodness of fit improves to a value of $r = 0.98$. The equation that describes this correlation is

$$\sigma_c = -0.3G \quad (6)$$

It is also evident from Fig. 12 that the relationship between shear modulus and axial compressive strength of graphite fibres can be described by Equation 6.

The microbuckling estimate given by the torsion modulus of PE is much higher than the measured compressive strength. The ratio of measured to predicted strength is only 0.13 for this fibre.

4. Discussion

The linear relationship between axial compressive strength and torsion modulus measured for the liquid-crystalline polymer and graphite fibres supports the

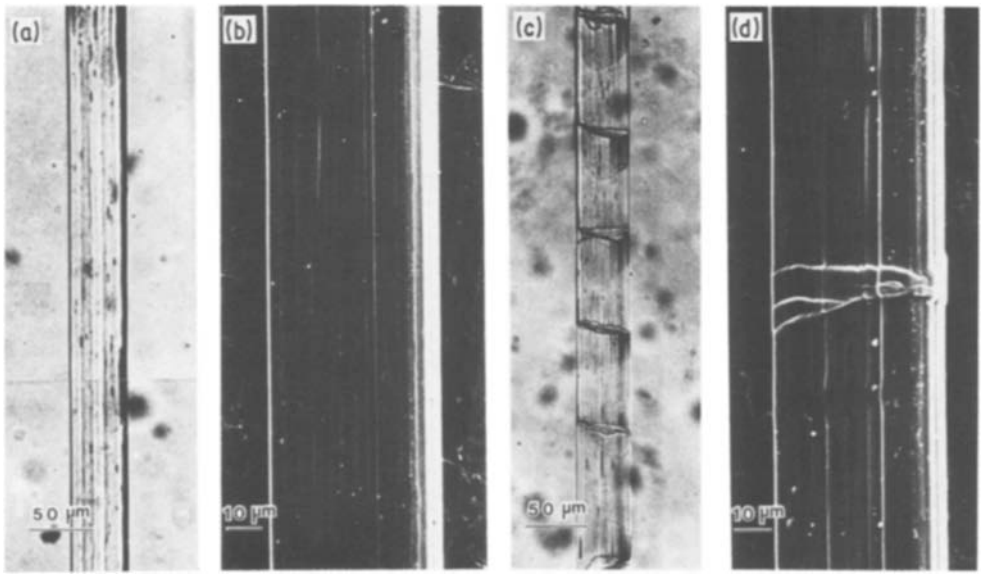

Figure 11 PE fibre. Before compression: (a) optical micrograph, (b) scanning electron micrograph. After compression: (c) optical micrograph, (d) scanning electron micrograph.

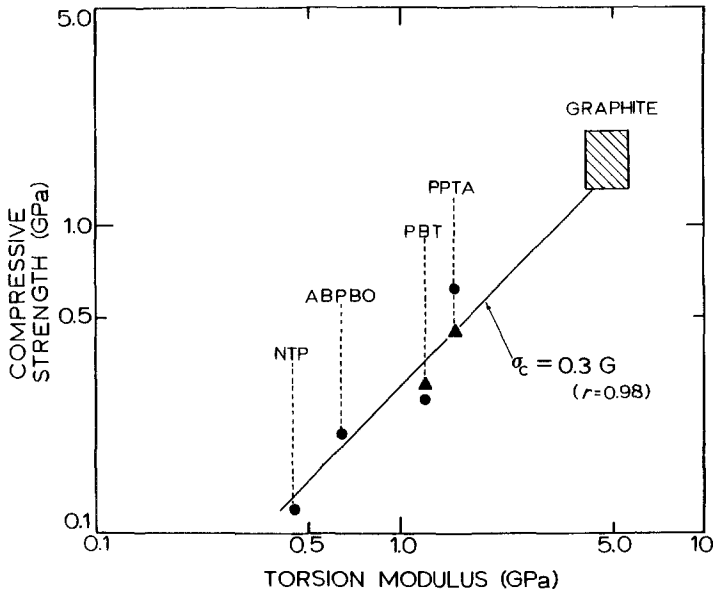

Figure 12 Plot of measured axial compressive strengths and torsion moduli for high performance organic fibres; (●) σ_c from single fibre tests, (▲) σ_c from composite data.

concept of compressive failure due to elastic microbuckling instabilities for these materials. The theoretical compressive strength was assumed to be identical to the longitudinal shear modulus measured from fibre torsion. For liquid-crystalline polymer and graphite fibres, the torsion moduli were essentially three times the corresponding measured compressive strengths. This disparity may be due to fibre anisotropy, voids, residual stresses and misalignment of polymer chains. The relationship of these factors to the microbuckling analysis for compressive strength has been discussed previously [7]; however, some of these factors will be reexamined here in greater detail.

Kevlar [32–34] and radial graphite fibres are cylindrically orthotropic and hence exhibit two longitudinal shear moduli: G_{rz} and $G_{\theta z}$. Torsion tests of fibres yield $G_{\theta z}$, which is the modulus of shearing between hydrogen-bonded sheets in Kevlar fibres and between basal planes in radial graphite fibres. Therefore, $G_{\theta z}$ is the lower longitudinal shear modulus for these fibres. The torsion modulus of "onion skin" graphite fibres is due to shearing within the basal planes and is larger than G_{rz}. Thus it is not surprising that reported torsion moduli of some graphite fibres [35, 36] are much greater than the value of 4.1 GPa determined for shear between dislocation-free graphite basal planes [30]. It must be emphasized that for fibres exhibiting an anisotropy such that $G_{\theta z} > G_{rz}$, the torsion modulus is the wrong estimate for the compressive strength of these materials.

Residual stresses have been shown to exist in graphite [37] and PBT fibres [38]. Indeed, the stresses generated during drying of PBT fibres are believed to be the cause of compressive kinking observed in the dried fibres [38]. Regions of a fibre that are under residual compression will reach critical buckling stresses first. Therefore, premature nucleation of kink bands can occur in such regions.

Although it is reasonable to assume the existence of residual stresses in all the fibres examined, these stresses must have minimal effect on the reduction in axial compressive strength. Significant residual stress would be indicated by a relatively large negative intercept on the plot of compressive strength against torsion modulus. The data plotted in Fig. 12 were fitted to a straight line which passed close to the origin, indicating only a small effect of residual stress on compressive strength. Another way in which large residual stresses could exist and affect the compressive strength relationship $\sigma_c = -0.3G$ is if the magnitude of the residual stress in each fibre was directly proportional to the torsion modulus. This is highly unlikely for the five different fibres studied. However, the presence of even small residual axial compressive stresses near the surface of these fibres could explain the initiation of kink bands there.

Small misalignment or curvature of chains and microfibrils should not affect the compressive stress that initiates elastic instabilities. However, under axial compression, these misaligned regions would be subjected to shear stresses that could possibly exceed the shear strength between chains or fibrils. Argon [16] has proposed that axial compressive strengths of fibre composites are limited by local shear failure along such planes of misalignment. He believes that shear failure initiates material collapse into a kink band. The longitudinal compressive strength of fibre composites that fail in this manner is given by

$$\sigma_c = \frac{\tau_m}{\phi} \tag{7}$$

where τ_m is the interlaminar shear strength and ϕ is the angle of misalignment measured with respect to load direction.

A fibre will always exhibit a distribution of chain orientation with shear failure occurring in the most poorly aligned regions. Although difficult to measure the largest misalignment angle based on Argon's proposal, it is reasonable to assume that fibres with better average orientation should have higher compressive strengths. However, the compressive strengths of PBT [29, 39] and Kevlar [28] fibres are relatively insensitive to the improvements in average axial orientation attained via tension heat-treatment. Thus, it appears unlikely that shear failure initiates compressive kink band formation in these fibres.

The gel-spun PE fibre does not obey the relationship between compressive strength and torsion modulus measured for the rigid rod polymer fibres. The existence of residual entanglements in PE fibres may severely limit their compressive strength.

As mentioned above for the Kevlar 49 and graphite fibres, it is necessary to measure the minimum longitudinal shear modulus to predict compressive strength. If the PE fibres are anisotropic within their cross-section, or if they contain amorphous regions that exhibit low shear moduli, then it is conceivable that the torsion modulus is not the best estimate of compressive strength.

Although it might be argued that a compressive buckling analysis should not apply to flexible polymer chains, it is emphasized that the analysis reveals that the critical compressive stress for microbuckling is a function only of intermolecular (or interfibrillar) interactions when the chains (or fibrils) are long. Therefore, the buckling stress for a collection of laterally interacting and infinitely flexible extended chains is also equal to the minimum longitudinal shear modulus of such a collection.

5. Conclusion

Analysis of a microbuckling model for the axial compressive failure of high performance polymer fibres yields a linear relationship between strength and longitudinal shear modulus. This relationship has been verified for liquid-crystalline polymer fibres and high modulus graphite fibres, which exhibit axial compressive strengths equal to 30% of their respective torsion moduli.

Acknowledgement

The authors acknowledge the generous support of this work by the Materials Laboratory of the Air Force, Wright Aeronautical Laboratories, and by the Office of Naval Research. We thank the following companies for supplying the fibre: E. I. DuPont de Nemours Co. for Kevlar, Allied-Signal Co. for PE, Celanese Co. for NTP and Union Carbide for P-75 graphite fibre.

References

1. S. J. DeTERESA, S. R. ALLEN, R. J. FARRIS and R. S. PORTER, *J. Mater. Sci.* **19** (1984) 57.
2. T. TAKAHASHI, M. MIURA and K. SAKURAI, *J. Appl. Polym. Sci.* **28** (1983) 579.
3. S. R. ALLEN, A. G. FILIPPOV, R. J. FARRIS, E. L. THOMAS, C-P. WONG, G. C. BERRY and E. C. CHENEVEY, *Macromol.* **14** (1981) 1135.
4. M. G. DOBB, D. J. JOHNSON and B. P. SAVILLE, *Polymer* **22** (1981) 960.
5. J. M. GREENWOOD and P. G. ROSE, *J. Mater. Sci.* **9** (1974) 1809.
6. M. M. SCHOPPEE and J. SKELTON, *Textile Res. J.* **44** (1974) 968.
7. S. J. DeTERESA, R. S. PORTER and R. J. FARRIS, *J. Mater. Sci.* **20** (1985) 1645.
8. H. M. HAWTHORNE and E. TEGHTSOONIAN, *ibid.* **10** (1975) 41.
9. E. OROWAN, *Nature* **149** (1942) 643.
10. K. SHIGEMATSU, K. IMADA and M. TAKAYANAGI, *J. Polym. Sci. Polym. Phys. Edn.* **13** (1975) 73.
11. M. S. PATERSON and L. E. WEISS, *Geol. Soc. Amer. Bull.* **77** (1966) 343.
12. N. C. GAY and L. E. WEISS, *Tectonophysics* **21** (1974) 287.
13. E. HONEA and A. M. JOHNSON, *ibid.* **30** (1976) 197.
14. C. W. WEAVER and J. G. WILLIAMS, *J. Mater. Sci.* **10** (1975) 1323.
15. C. R. CHAPLIN, *ibid.* **12** (1977) 347.
16. A. S. ARGON, in "Treatise on Materials Science and Technology", Vol. 1, edited by H. Herman (Academic, New York, 1972) p. 79.
17. A. G. EVANS and W. F. ADLER, *Acta Metall.* **26** (1978) 725.
18. L. E. WEISS, *Tectonophysics* **65** (1980) 1.
19. R. E. ROBERTSON, *J. Polym. Sci. A-2* **7** (1969) 1315.
20. H. BLADES, US Patent 3 869 430, assigned to E. I. DuPont de Nemours Co. (1975).
21. P. SMITH and P. LEMSTRA, *J. Mater. Sci.* **15** (1980) 505.
22. R. J. DIEFENDORF and E. TOKARSKY, *Polym. Eng. Sci.* **15** (1975) 150.
23. W. N. REYNOLDS, in "Chemistry and Physics of Carbon", Vol. II, edited by P. L. Walker, Jr and P. A. Thrower (Marcel Dekker, New York, 1973) p. 2.
24. W. R. JONES and J. W. JOHNSON, *Carbon* **9** (1971) 645.
25. A. J. PERRY, B. INEICHEN and B. ELIASSON, *J. Mater. Sci. Lett.* **9** (1974) 1376.
26. ASTM D3379-75e, ASTM, Philadelphia (1975).
27. S. J. DeTERESA, R. S. PORTER and R. J. FARRIS, *Polym. Comp.* **2** (1982) 57.
28. R. E. WILFONG and J. ZIMMERMAN, *J. Appl. Polym. Sci. Appl. Polym. Symp.* **31** (1977) 1.
29. J. F. MAMMONE and W. C. UY, Air Force Technical Report, AFML-TR-82-4154 (1984).
30. E. J. SELDIN and C. W. NEZBEDA, *J. Appl. Phys.* **41** (1970) 3389.
31. D. W. HADLEY, P. R. PINNOCK and I. M. WARD, *J. Mater. Sci.* **4** (1969) 152.
32. M. G. DOBB, D. J. JOHNSON and B. P. SAVILLE, *J. Polym. Sci. Polym. Phys. Edn.* **15** (1977) 2201.
33. R. HAGEGE, M. JARRIN and M. J. SOTTON, *J. Microsc. O.* **115** (1979) 65.
34. S. B. WARNER, *Macromol.* **16** (1983) 1546.
35. R. BACON, in "Chemistry and Physics of Carbon", Vol. 9, edited by P. L. Walker Jr and P. A. Thrower (Marcel Dekker, New York, 1973) p. 80.
36. J-B. DONNET and R. C. BANSAL, in "Carbon Fibers" (Marcel Dekker, New York, 1984) p. 171.
37. K. CHEN, C. W. LeMAISTRE, J. H. WANG and R. J. DIEFENDORF, 182nd National Conference, ACS, Poly 137, New York, August (1981).
38. S. R. ALLEN, A. G. FILIPPOV, R. J. FARRIS and E. L. THOMAS, *J. Appl. Polym. Sci.* **26** (1981) 291.
39. S. R. ALLEN, PhD thesis, University of Massachusetts, Amherst (1983).

Received 12 March
and accepted 15 May 1987